Atmospheric Research 183 (2017) 42–57

Contents lists available at ScienceDirect

Atmospheric Research

journal homepage: www.elsevier.com/locate/atmosres

A multi-sensor study of the impact of ground-based glaciogenic seeding on clouds and precipitation over mountains in Wyoming. Part II: Seeding impact analysis

Binod Pokharel [a,*], Bart Geerts [a], Xiaoqin Jing [a], Katja Friedrich [b], Kyoko Ikeda [c], Roy Rasmussen [c]

[a] Department of Atmospheric Science, University of Wyoming, Laramie, WY 82071, USA
[b] Department of Atmospheric and Oceanic Sciences, University of Colorado, Boulder, CO 80309, USA
[c] Research Application Laboratory, National Center for Atmospheric Research, Boulder, CO 80307, USA

ARTICLE INFO

Article history:
Received 4 May 2016
Received in revised form 10 August 2016
Accepted 20 August 2016
Available online 23 August 2016

Keywords:
Glaciogenic seeding
Orographic cloud and precipitation
Radar reflectivity
Airborne measurements

ABSTRACT

The AgI Seeding Cloud Impact Investigation (ASCII) campaign, conducted in early 2012 and 2013 over two mountain ranges in southern Wyoming, was designed to examine the impact of ground-based glaciogenic seeding on snow growth in winter orographic clouds. Part I of this study (Pokharel and Geerts, 2016) describes the project design, instrumentation, as well as the ambient atmospheric conditions and macrophysical and microphysical properties of the clouds sampled in ASCII. This paper (Part II) explores how the silver iodide (AgI) seeding affects snow growth in these orographic clouds in up to 27 intensive operation periods (IOPs), depending on the instrument used.

In most cases, 2 h without seeding (NOSEED) were followed by 2 h of seeding (SEED). In situ data at flight level (2D-probes) indicate higher concentrations of small snow particles during SEED in convective clouds. The double difference of radar reflectivity Z (SEED − NOSEED in the target region, compared to the same trend in the control region) indicates an increase in Z for the composite of ASCII cases, over either mountain range, and for any of the three radar systems (WCR, MRR, and DOW), each with their own control and target regions, and for an array of snow gauges. But this double difference varies significantly from case to case, which is attributed to uncertainties related to sampling representativeness and to differences in natural trends between control and target regions. We conclude that a sample much larger than ASCII's sample is needed for clear observational evidence regarding the sensitivity of seeding efficacy to atmospheric and cloud conditions.

1. Introduction

This is the second part of an observational study that explores whether a measurable signal of ground-based glaciogenic seeding can be detected, in terms of ice crystal size distribution and mainly snowfall rate. Pokharel and Geerts (2016, hereafter referred to as Part I) describes the AgI Seeding Cloud Impact Investigation (ASCII) experimental design, as well as the characteristics of the sampled orographic clouds, flow field, and upstream stability profiles in ASCII's 27 intensive operation periods (IOPs). A map of the terrain, the facilities deployed in ASCII, and the flight track of the University of Wyoming King Air (UWKA) is shown in Fig. 1. This paper (Part II) compares particle size distributions, precipitation rates, and mainly radar reflectivity profiles for all these IOPs. Comparison are drawn both spatially (target vs. control regions) and temporally (SEED vs. NOSEED).

Comparisons using three different radar systems are described in Section 2, and comparisons based on particle probe data are made in Section 3. The impact of seeding is estimated in Section 4, using double differences based on these radar systems as well as snow gauges. Caveats and suggestions for improvements are discussed in Section 5. The findings are summarized in Section 6.

2. Change in radar reflectivity

This section examines the change in reflectivity from NOSEED to SEED periods for three different radar systems, each with their own target and control regions. These are the W-band (3 mm) airborne profiling Wyoming Cloud Radar (WCR), the volume-scanning X-band (3 cm) Doppler on Wheels (DOW) radar, and a pair of profiling Ka-band (1.2 cm) Micro Rain Radars (MRRs), all described in Part I. We start with composite reflectivity profiles from the WCR, based on all available ASCII IOPs, listed in Table 1 in Part I. First we define the control region as the flight leg upwind of the AgI generators (leg 1 in Fig. 1) and the target

Abbreviations: ZIP, reflectivity impact factor; PIF, precipitation impact factor; ASCII, AgI Seeding Cloud Impact Investigation; UWKA, University of Wyoming King Air; WCR, Wyoming Cloud Radar; WCL, Wyoming Cloud Lidar; MRR, Micro-Rain Radar; DOW, Doppler on Wheels.

* Corresponding author at: Department of Atmospheric Science, University of Wyoming, Laramie, WY 82072, USA.
E-mail address: bpokhare@uwyo.edu (B. Pokharel).

http://dx.doi.org/10.1016/j.atmosres.2016.08.018
0169-8095/

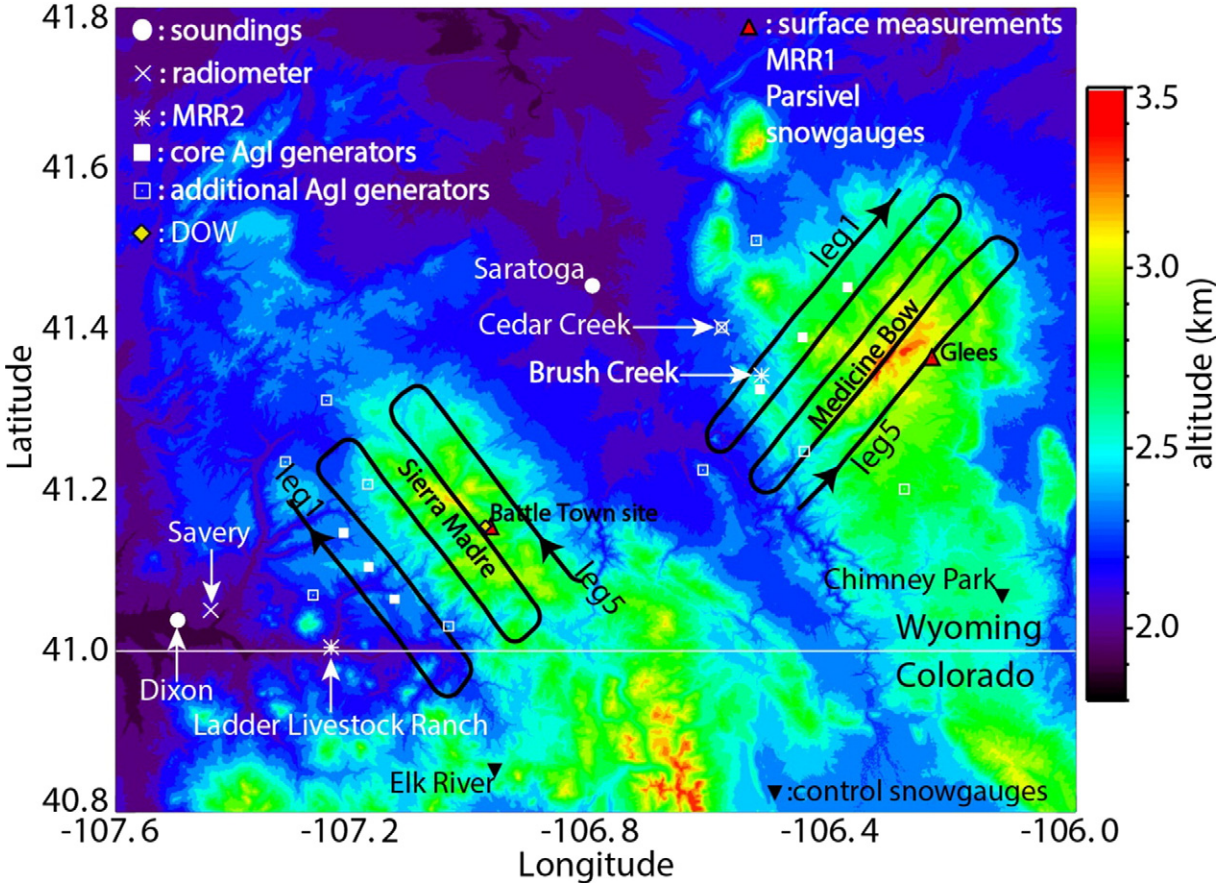

Fig. 1. Terrain map and ASCII deployment map over the Sierra Madre (SM) and Medicine Bow (MB) Mountains in southern Wyoming. The solid black lines show the fixed UWKA flight tracks and square symbols show the ground-based AgI generators. The three most commonly used AgI generators are shown by the filled squares.

region as the four downstream legs (Section 2.1). Next, to build evidence that differences are seeding-related, we contrast temporal changes inside dispersion plumes (target) against those outside (control) (Section 2.2). We also contrast Medicine Bow (MB) vs. Sierra Madre (SM) (Section 2.3), and convective vs. stratiform clouds (Section 2.4). Finally, we evaluate the reflectivity changes from NOSEED to SEED for the MRR pair (Section 2.5) and for the DOW (Section 2.6).

2.1. Target and control WCR reflectivity

A seeding signature is not immediately obvious in the reflectivity pattern downwind of AgI generators in any IOP. Therefore the WCR reflectivity profiles are composited for all flight legs in the form of frequency-by-altitude displays (FADs) (Yuter and Houze, 1995). The frequency is normalized, such that any number of transects can be added, and the sum of all counts (all heights, all reflectivity bins) equals 100%. The height is expressed above ground level (AGL) because AgI seeding is ground-based and, to a first order, low-level tracers are advected over the terrain, roughly following the terrain contour. The FAD approach has been used in several ASCII case studies (Pokharel et al., 2014a, 2014b, 2015). Here we use it for the composite of all available cases: the WCR reflectivity FAD for 21 ASCII IOPs is shown in Fig. 2. This includes nine IOPs over the SM and 12 IOPs over the MB. Three IOPs in pre-ASCII (10, 25 and 30 March 2009) are excluded because no control measurements were collected (Table 1 in Part I).

WCR reflectivity data from the target tracks (legs 2–5) and the control track (leg 1) are composited during NOSEED and SEED (Fig. 2). In most IOPs NOSEED preceded SEED, enabling a rapid transition between the two periods, although the UWKA flew one or two cross-mountain along-wind legs between the two periods (*e.g.*, Fig. 4 in Part I), to allow AgI nuclei to disperse. Both periods usually contain two full ladders of five legs (Fig. 1), and thus the WCR sample size of SEED is about the same as that of NOSEED. As can be seen in the cumulative distance listed in the upper four panels of Fig. 2, the SEED sample size is 15–20% smaller on average than the NOSEED sample size in both regions. This is because in some IOPs the aircraft was unable to complete the 4th ladder (part of SEED), and in some cases the wind was not strong enough for the first leg flown on ladder 3 (leg 5, furthest downwind, Fig. 1) to be counted as part of SEED. The exact start and end times for NOSEED and SEED are listed in Table 1 in Part I.

The dip in the "data presence" line between 1 and 2 km AGL in all upper four panels in Fig. 2 is an artifact due to the radar blind zone (*e.g.*, Fig. 4 in Part I). It gives an indication of the typical flight level AGL. The average reflectivity is computed in Z units ($mm^6\ m^{-3}$) and expressed in dBZ in Fig. 2. It is converted to precipitation rate R ($mm\ h^{-1}$) in the upper abscissa of the two lower panels of Fig. 2 using:

$$R = aZ^b \tag{1}$$

For the WCR we use $a = 0.39$, and $b = 0.58$ in Eq. (1), based on Pokharel and Vali (2011), who use WCR data collected over and near the MB range. This is close to the Z–R relationship derived theoretically for mm-wavelength radar by Matrosov (2007). The uncertainty in these relationships is large (larger than factor of two), mainly because of the uncertainty in ice particle density, which is strongly affected by riming. For the MRR and the DOW radars, we use $a = 0.046$, and $b = 0.67$ in Eq. (1), based on Matrosov et al. (2009). The precipitation rate in Fig. 2 is a conditional rate, *i.e.* when it is snowing. The fraction of time it was snowing at any height can be estimated from the data presence line.

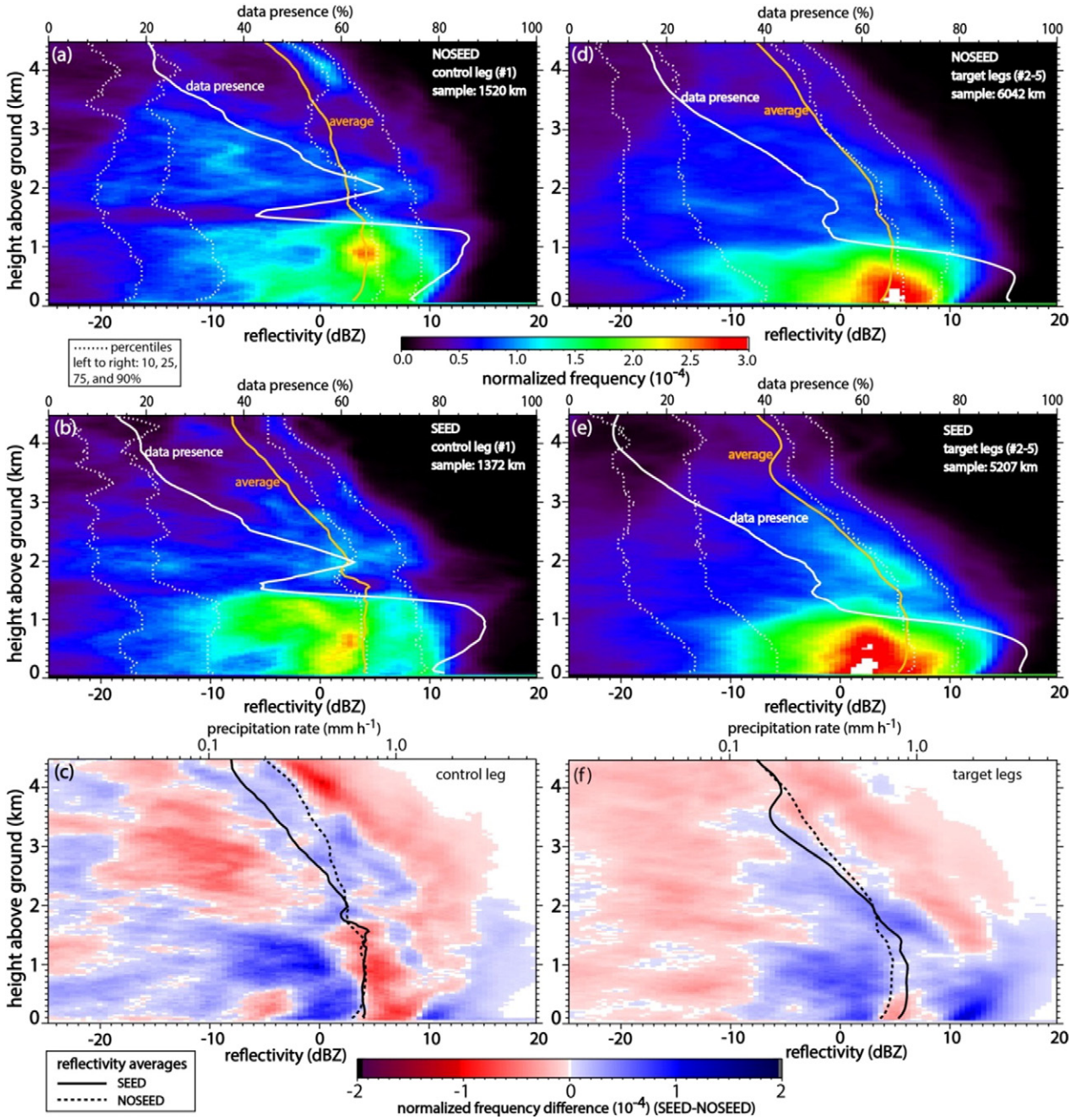

Fig. 2. Normalized frequency-by-altitude displays of WCR reflectivity for 21 flights, *i.e.* nine in ASCII-12 over the SM, and eight in ASCII-13 plus four in pre-ASCII, both over the MB. The right panels apply to the four tracks downwind of the AgI generators (target), and the left panels to leg 1 upstream of the generators (control) (Fig. 1). The top panels apply to the NOSEED period, the middle panels to the SEED period, and the bottom panels show the difference (SEED − NOSEED). The sample size for the upper four FADs is expressed in terms of UWKA flight distance (one sample per ~4 m). The dotted lines in the upper four FADs are the 10th, 25th, 75th, and 90th percentiles. Also shown are the mean reflectivity profiles (orange lines in the upper four panels, and black lines in the bottom panels) and the "data presence", *i.e.* the percentage of WCR range gates with a WCR echo as a function of height (white line in the upper four panels). The precipitation rate (R) shown in the upper abscissa of the bottom panels is inferred from $R = 0.39\,Z^{0.58}$.

The data presence is suppressed near the surface in the control region (foothills), compared to the target region (over the mountain), where significant reflectivity values (>0 dBZ) near the surface are far more common (Fig. 2a and d). Also, the average low level reflectivity is 1–2 dBZ smaller in the control region compared to the target region during NOSEED. These are orographic effects, *i.e.* snow grows at low levels above the LCL (Table 1 in Part I) over the mountain. Echoes are often elevated (not reaching the ground) along leg 1, as can be seen on the west side of the transects in Figs. 4 and 5 in Part I. Fig. 2 also confirms that storms sampled in ASCII were quite shallow, with echoes present at 4 km AGL <20% of the time on average.

We now compare two periods, SEED vs. NOSEED, for the composite of 21 IOPs. The average low-level reflectivity remains the same from NOSEED to SEED in the control region (Fig. 2c), but it increases in the target regions from NOSEED to SEED (Fig. 2f): in the lowest 1.5 km the average reflectivity is ~1.5 dBZ larger during SEED, which corresponds with a ~30% increase of the precipitation rate, according to Eq. (1). This increase is largely due to an increased frequency of strong (>10 dBZ) echoes at low levels during SEED in the target region.

This increase cannot be attributed to storm deepening during SEED: the upper-level (>2 km AGL) mean reflectivity and data presence in fact is generally lower during SEED in the target region (Fig. 2). The same

weakening aloft, from NOSEED to SEED, is found in the control region: the structure of the two difference FADs in Fig. 2c and f is similar (*i.e.* the red–blue–red sequence at upper levels), indicating that the natural storm trend above the seeded boundary-layer was similar in target and control regions. In some IOPs the storm weakened, in other cases reflectivity above the PBL tended to increase from NOSEED to SEED periods. The net effect for 21 IOPs is a slight weakening aloft.

2.2. WCR reflectivity: comparison with a lateral control region

To further explore the possibility that the low-level change in WCR reflectivity is due to AgI seeding, we contrast changes in the sections of flight legs assumed to be within a AgI plume downwind of a generator, against the section believed to be outside any plume. We do this mainly because lateral control, over similar terrain, is more representative than upwind control, over the foothills: for instance, an increase in stability and/or decrease in wind speed tends to shift orographic precipitation upwind of the mountain (*e.g.*, Houze, 2012). Also, the upwind control region is rather small (1 flight leg) compared to the target region (4 legs). The drawback of the lateral control approach is that the AgI dispersion plumes were not measured independently (*e.g.* by releasing an inert tracer from the AgI generator sites, and measuring its concentration downwind). There is some evidence that AgI seeding plumes tend to be rather narrow, both from observations (Holroyd et al., 1988; Huggins, 2007) and from modeling work (Xue et al., 2014). We can be fairly confident that under the rather low-stability, high-wind conditions observed in ASCII (see Part I), the AgI dispersion plumes are almost always contained within a cone confined by $\pm 10°$ of the mean low-level wind direction from the left- and right-most generators. The flight sections within this box ("target") are shown in the insert map in Fig. 3a. The flight sections outside this box ("lateral control") are shown in the insert map in Fig. 3b. Only the 20 IOPs with two or three AgI generators in operation are used for this analysis (Table 1 in Part I). This approach allows a more balanced sampling in

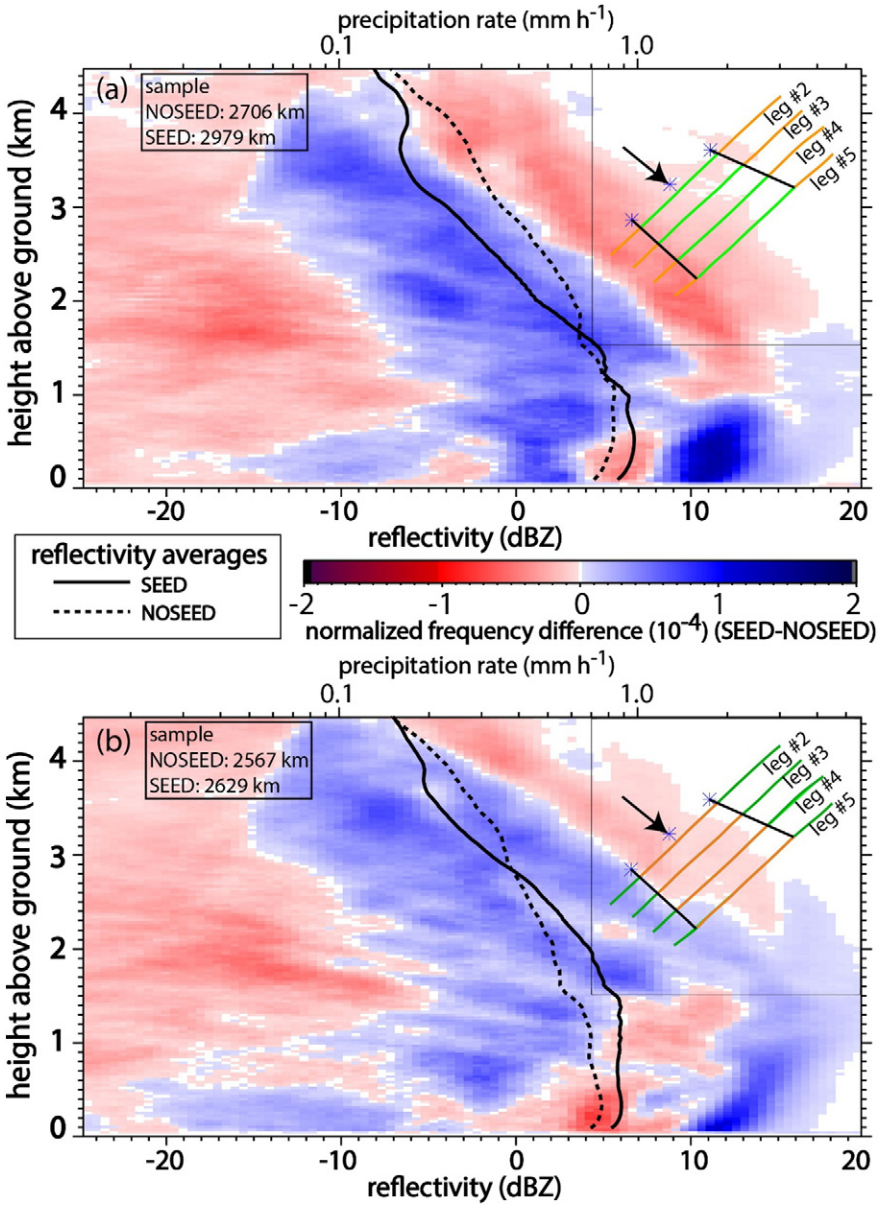

Fig. 3. WCR reflectivity difference (SEED minus NOSEED) FADs for the target legs (2–5) for all three-generator IOPs (20 flights) a) within the assumed AgI dispersion cones (shown schematically as green track portions in the insert map) and b) outside this region. The insert maps also show the location of the three AgI generators (blue asterisks), the wind direction (arrow), and the sample size (km). The orientation of the cones varies with the mean wind direction for each IOP.

the target region (51% of the composite flight track length) vs. the lateral control region (49%) during SEED and NOSEED. There is a chance of course that the lateral control region occasionally is impacted by seeding especially for low Froude number or high wind shear cases.

A higher frequency of enhanced reflectivity during SEED is observed both inside the target cone and the lateral control region (Fig. 3). But this increase in reflectivity is mainly aloft in the lateral control region, and mainly below 1 km within the target cone. The near-surface dipole of increased chances of high reflectivity values (~11 dBZ) and decreased chances of slightly lower reflectivity values (~6 dBZ) within the target cone is striking (Fig. 3a). This suggests that the observed low-level reflectivity increase in the target region, compared to the corresponding change in the upwind control region (Fig. 2c and f), arises mostly from changes immediately downwind of the AgI generators. It is one piece of evidence suggesting that ground-based seeding increases radar reflectivity. This piece of evidence will become clearer in Section 4, where we introduce a double ratio.

2.3. WCR reflectivity: Medicine Bow versus Sierra Madre

The orographic clouds sampled over the MB were ~5 K colder than those over the SM (Fig. 3 in Part I). Do the findings from the composite analysis (Fig. 2) apply to both mountains individually? The WCR reflectivity is higher during SEED compared to NOSEED both in the (upwind) control and target regions over the MB (Fig. 4a and b), suggesting storm intensification from NOSEED to SEED. However, the opposite applies for the SM cases: the reflectivity is lower during SEED in both regions (Fig. 4c and d), suggesting storm decay. Natural trends vary widely from one IOP to another. But the SEED–NOSEED increase (decrease) in low-level reflectivity in the target region compared to the control region is larger (smaller) over the MB (SM). If we consider the change in the control region as natural variability, and the change in target region is natural variability plus seeding impact, then the WCR reflectivity data suggest a positive seeding impact over both mountains.

2.4. WCR reflectivity: convective versus stratiform clouds

The impact of ground-based seeding on snow growth may depend on cloud type. The AgI nuclei are mixed only within the turbulent PBL in stratiform cases, while convection may carry seeding material to higher levels. To analyze the effect of cloud type, the 21 IOPs used for Fig. 2 are grouped into convective and stratiform types of cloud (Table 1 and Section 3.3, both in Part I). Six of these 21 IOPs are classified as convective, and the remaining 15 are stratiform. The (upwind) control (leg 1) and target (legs 2–5) regions are the same for all cases.

The target region shows enhanced low-level reflectivity during SEED for both cloud types (Fig. 5a and c), with a higher probability of strong (>10 dBZ) echoes near the surface, especially for stratiform clouds. The corresponding trend in the control region is rather insignificant for both cloud types (Fig. 5b and d), with a slight weakening in convective cases. (The spike at 1.5 km AGL in Fig. 5b is an artifact due to the radar blind zone, resulting in very few data near that level.) The low-level reflectivity difference (SEED — NOSEED) in the target region, compared to the corresponding difference in the control region, is about the same for both cloud types: this double difference (introduced in Section 4 below) is 1.4 dB when averaged over the lowest 1 km AGL. This WCR-based finding is consistent with a DOW analysis of fewer ASCII cases for stratiform (Jing et al., 2015) and convective (Jing and Geerts, 2015) clouds. It is possible that a larger positive response would emerge from the convective cases, if the target region was to extend further in the lee than leg 5 (Fig. 1), since most precipitation in these cases fell in the lee (Section 4.2 in Part I).

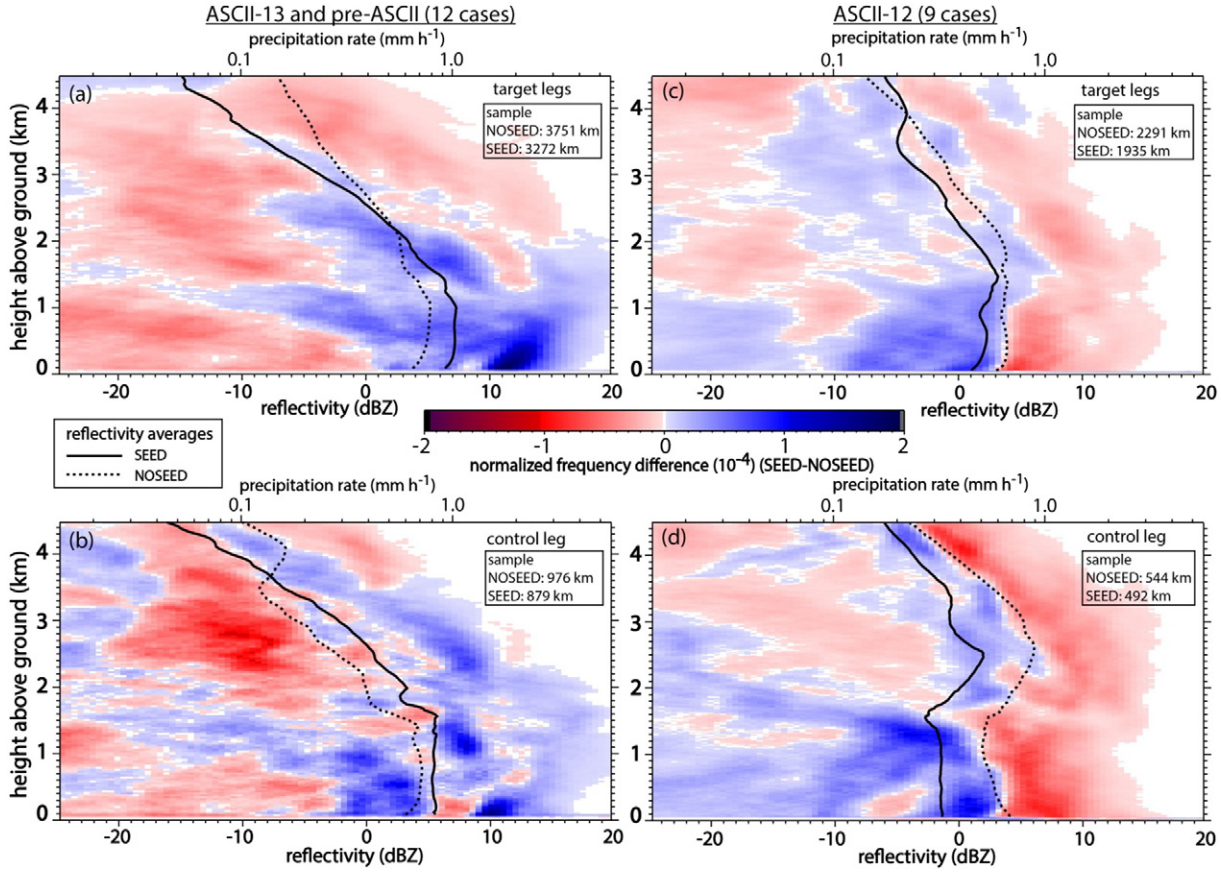

Fig. 4. WCR reflectivity difference (SEED minus NOSEED) FADs for the 12 flights over the MB (left panels) and for the nine flights over the SM (right panels). The target region is shown in the upper panels, the control region in the lower panels. The solid and dotted lines show the average values during SEED and NOSEED, respectively.

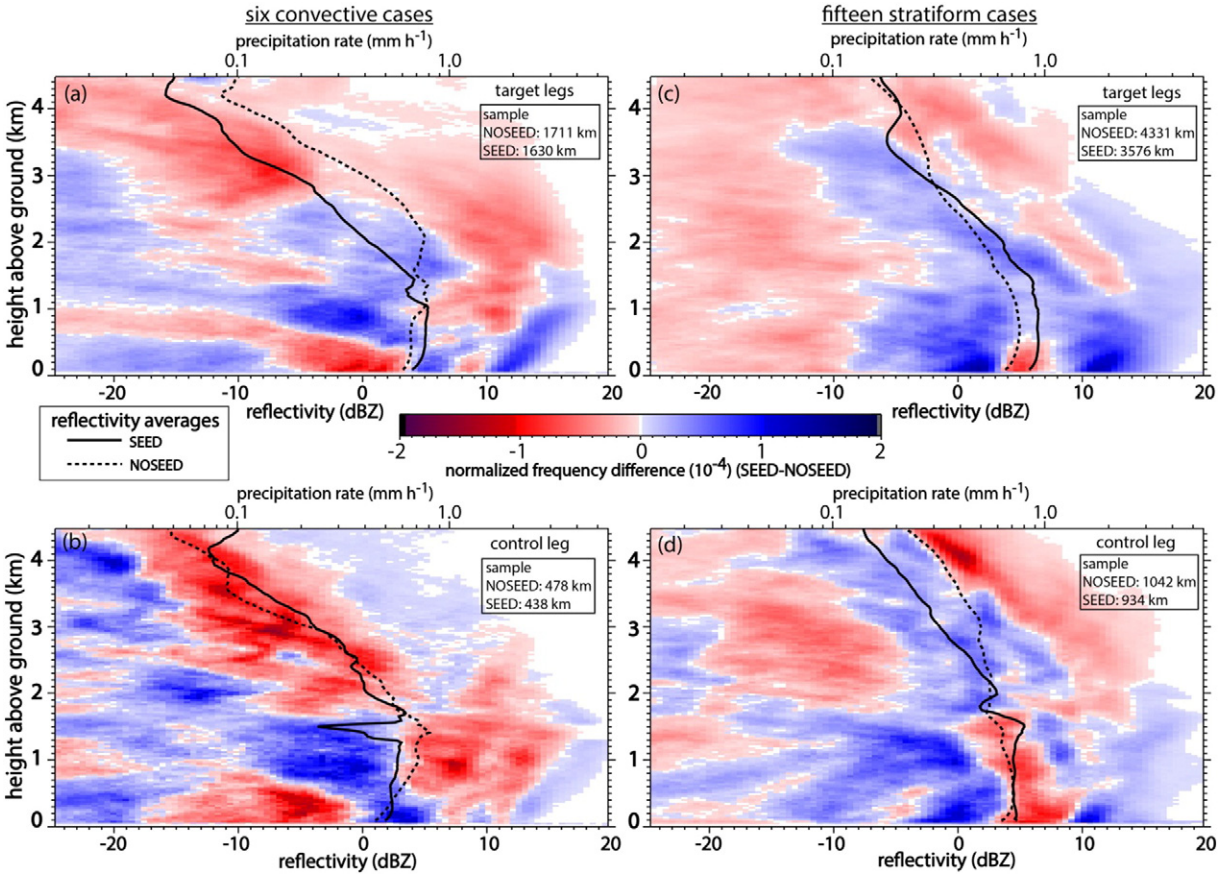

Fig. 5. WCR reflectivity difference (SEED minus NOSEED) FADs for six convective cloud IOPs (left panels) and for 15 stratiform cloud IOPs (right panels), for the target region (upper panels) and the control region (lower panels).

2.5. Target and control MRR reflectivity

Two MRRs were deployed in ASCII-12, one upstream of the AgI generators, and one downstream, at Battle Town site in the SM (Fig. 1). MRR reflectivity profiles at Battle Town site can be used to analyze seeding impact only if the site is impacted by the AgI plume. Evidence for this impact comes from two methods, (1) wind direction and (2) concentration of silver (Ag) and other trace elements in freshly fallen snow samples at Battle Town site. The predicted plume advection pattern is based on the average wind direction between the surface and mountain top level, using one or more upwind soundings during SEED. The minimum distance between the plume's center and Battle Town site is calculated, for any active AgI generator. The smaller this distance, the more likely it is that snow grown between the source and Battle Town site is impacted by AgI. The Ag concentration in the snow samples collected during SEED (relative to the NOSEED baseline concentration) is compared with the minimum distance to the closest plume center (Fig. 6).

The Ag concentration increase in snow samples collected during SEED is insignificant or negative when the minimum distance is large (>4 km). All but two cases (February 10 and 21) do show a more-than-doubling of the Ag concentration during SEED when the minimum distance is small (<4 km). There are many possible reasons for the two exceptions, but we can only speculate. Certainly the number of snow samples during SEED was small in both cases, as the snowfall rate was light. This confirms that when the predicted AgI plume is not far from Battle Town site, the snow sample reveals a higher Ag concentration during SEED.

The analysis in Fig. 6 yields eight IOPs (out of 12) suitable for the seeding impact analysis of data collected at Battle Town site, *i.e.* those IOPs with a minimum distance <4 km. The two IOPs for which the Ag concentration does not more-than-double are included as well, essentially because we have little faith in the Ag measurements in these two cases. The eight IOPs are listed in Table 1. The first two cases in this table (January 18 and 19) do not have data for the upstream MRR, so only six cases are considered for the dual-MRR analysis.

The MRR data are reprocessed to reduce noise, following Maahn and Kollias (2012). Except during heavy snowfall, the first two range gates had to be discarded, thus the effective minimum data level for the reflectivity FAD is 450 m AGL for the MRR at Battle Town site, and 700 m for the upwind valley MRR, whose gate spacing was larger. The

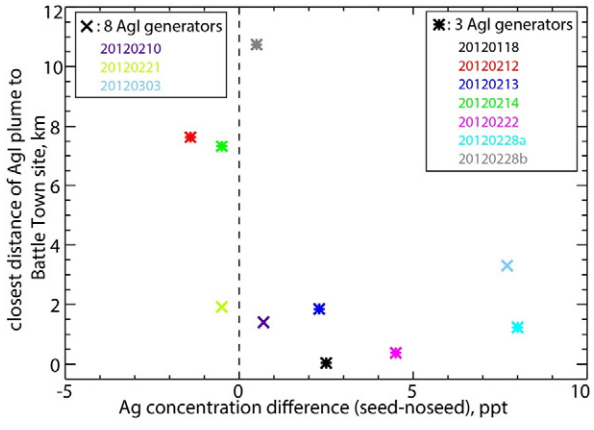

Fig. 6. Silver (Ag) concentration difference in snow samples (SEED minus NOSEED) as a function of the nearest distance between the estimate AgI plume center and the snow collection site (Battle Town site). The asterisks show the three-generator IOPs, and the crosses show the eight-generator IOPs.

Table 1
ASCII IOPs for which data from the MRR pair, the Parsivel disdrometer, and/or the gauges can be used in the seeding impact analysis, based on the wind direction and silver concentration in snow. Also shown are the NOSEED and SEED periods for these instruments. The last column lists the IOPs that can be used for DOW-based seeding impact analysis.

Range	IOP date (YYYY/MM/DD)	NOSEED UTC (HHMM)		SEED UTC (HHMM)		MRR		Parsivel	Snow gauge		DOW
		Start	Stop	Start	Stop	Target	Control	Target	Target	Control	
Sierra Madre	2012/01/18	0000	0145	0146	0346	Y	N	Y	N	N	N
	2012/01/19	1623	1826	1827	2030	Y	N	Y	Y	N	Y
	2012/02/11	0213	0518	0519	0824	Y	Y	Y	Y	Y	Y
	2012/02/12										Y
	2012/02/13	1900	2100	2101	2300	Y	N	Y	Y	Y	Y
	2012/02/21	1918	2139	2140	2538	Y	Y	Y	Y	Y	Y
	2012/02/22	1327	1527	1528	1728	Y	Y	Y	Y	Y	Y
	2012/02/28a	1331	1527	1528	1724	Y	Y	Y	Y	Y	Y
	2012/02/28b										Y
	2012/02/29										Y
	2012/03/03	1730	1956	1957	2223	Y	Y	Y	Y	Y	Y
Medicine Bow	2013/01/29	2159	2359	2400	2600				Y	Y	
	2013/02/01	1830	2030	2031	2231				Y	Y	
	2013/02/28	0000	0210	0211	0425				Y	Y	
	2009/02/18	1630	1830	1831	2031				Y	Y	
	2009/03/25	1515	1715	1716	1931				Y	Y	

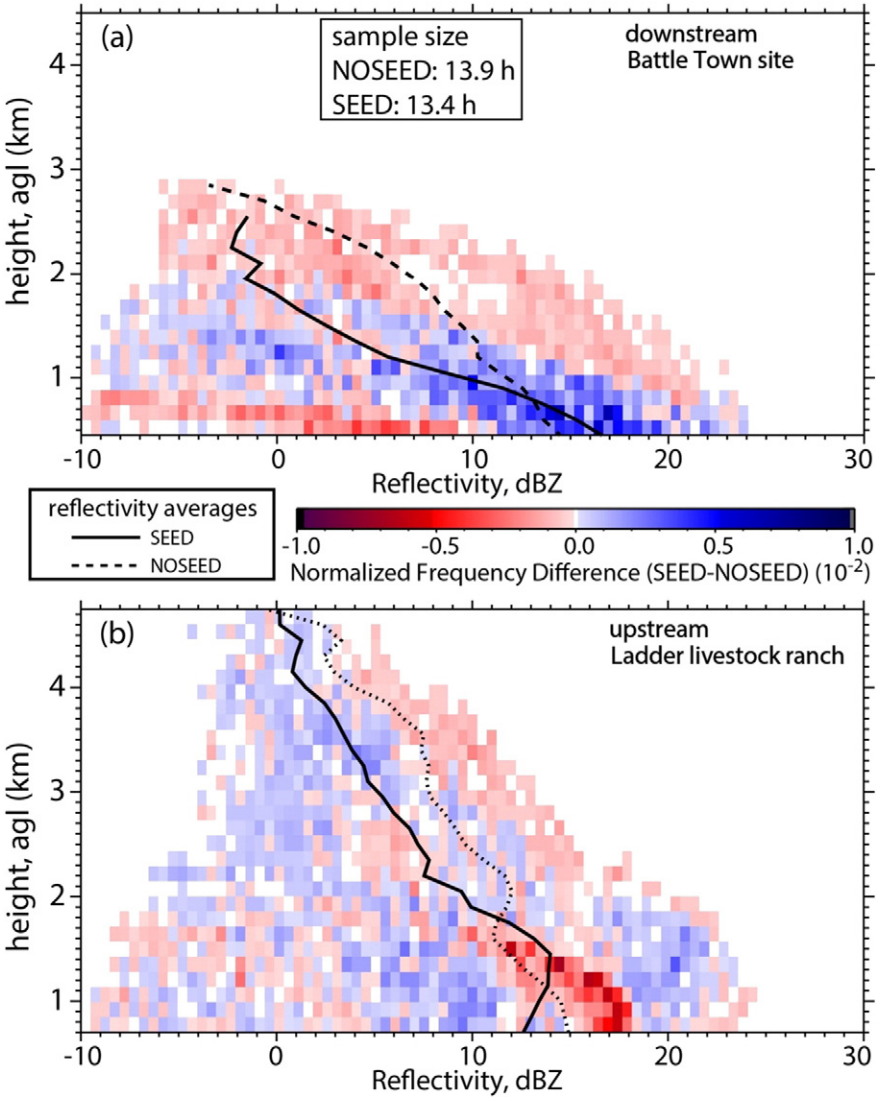

Fig. 7. MRR reflectivity difference (SEED minus NOSEED) FADs for a) the downstream MRR (target) and b) the upstream MRR (control), for six ASCII-12 cases (Table 1). The sample size applies to both MRR sites.

MRRs are less sensitive than the WCR (minimum detectable echo at a range of 1 km is ~−8 dBZ for the MRR, vs ~−25 dBZ for the WCR), but the larger particles scatter more strongly, because the size boundary between Mie and Rayleigh scattering is four times larger. Thus for heavy snowfall any *Z–R* relationship applies better at Ka-band (and *a fortiori* at X-band) than at W-band.

The SEED minus NOSEED reflectivity FADs composited for these six IOPs are shown in Fig. 7 for the downstream MRR (top panel) and the upstream MRR (bottom panel). The mean vertical reflectivity gradient at the downstream site (solid or dashed lines in Fig. 7a) is rather high, due to subsidence aloft and low-level snow growth below. This gradient is smaller at the upstream site (Fig. 7b), as echoes tend to be deeper at the upstream site (the foothills region), and in fact low-level sublimation may occur, producing an elevated *Z* maximum. [See Figs. 4 and 5 in Part I for examples, and Geerts et al. (2015a) for a detailed discussion of this orographic effect.]

The NOSEED and SEED periods for the MRR analysis (Table 1) are slightly different from those for the WCR (Table 1 in Part I). For all IOPs, NOSEED is defined as an equally long period as SEED, which is the actual seeding period adjusted for the typical advection time between the AgI source and Battle Town site. The target MRR did not work for ~30 min during SEED in one IOP (21 February 2012), so the MRR's SEED sample size is slightly smaller than the NOSEED sample size (Fig. 7). The upstream MRR composite reflectivity FAD shows that, on average, storms were weakening between NOSEED and SEED, both aloft and at low levels (Fig. 7b). The same weakening is evident above the PBL at the target site impacted by AgI seeding (Fig. 7a), except in the lowest 0.8 km AGL.

If the MRR NOSEED period is defined as a longer, two-part period straddling the (typically two-hour long) SEED period, with a one-hour buffer period after SEED, then the six-storm composite SEED − NOSEED reflectivity difference FAD still shows a somewhat lesser storm intensity during SEED at the upstream control site, while the difference FAD at the target site still reveals a higher mean reflectivity at low levels during SEED (not shown), consistent with Fig. 7.

2.6. Target and control DOW reflectivity

A DOW radar located at Battle Pass (Fig. 1) conducted volume scans at 10 min intervals during the ASCII-12 IOPs. Battle Pass affords excellent low-level coverage to the W and E-NE, but higher terrain along the crest to the NW and especially to the SE results in poor low-level coverage in those sectors (Fig. 8a). Two control areas can be used for the DOW. An upwind control region is intended to capture precipitation areas moving towards Battle Pass. It is defined as an area generally upwind of the AgI generators with lowest-elevation DOW data no > 1.0 km AGL (Fig. 8a). When only the three core AgI generators were used, the upwind control region was confined on the sides by the wind direction, as shown by black lines in Fig. 8b, and as described in more detail in Jing et al. (2015). The lateral control region, designed to represent conditions over the mountain, but to the side of the AgI plumes, is outside these black lines, in an area over the mountain with reasonable low-level coverage (lowest beam <1 km AGL). Lateral control applies only to IOPs with just three generators. Finally, the target is a region downwind of the AgI generators, stretching ~18 km downwind of Battle Pass (Fig. 8a). The DOW's low-level coverage is excellent in the target

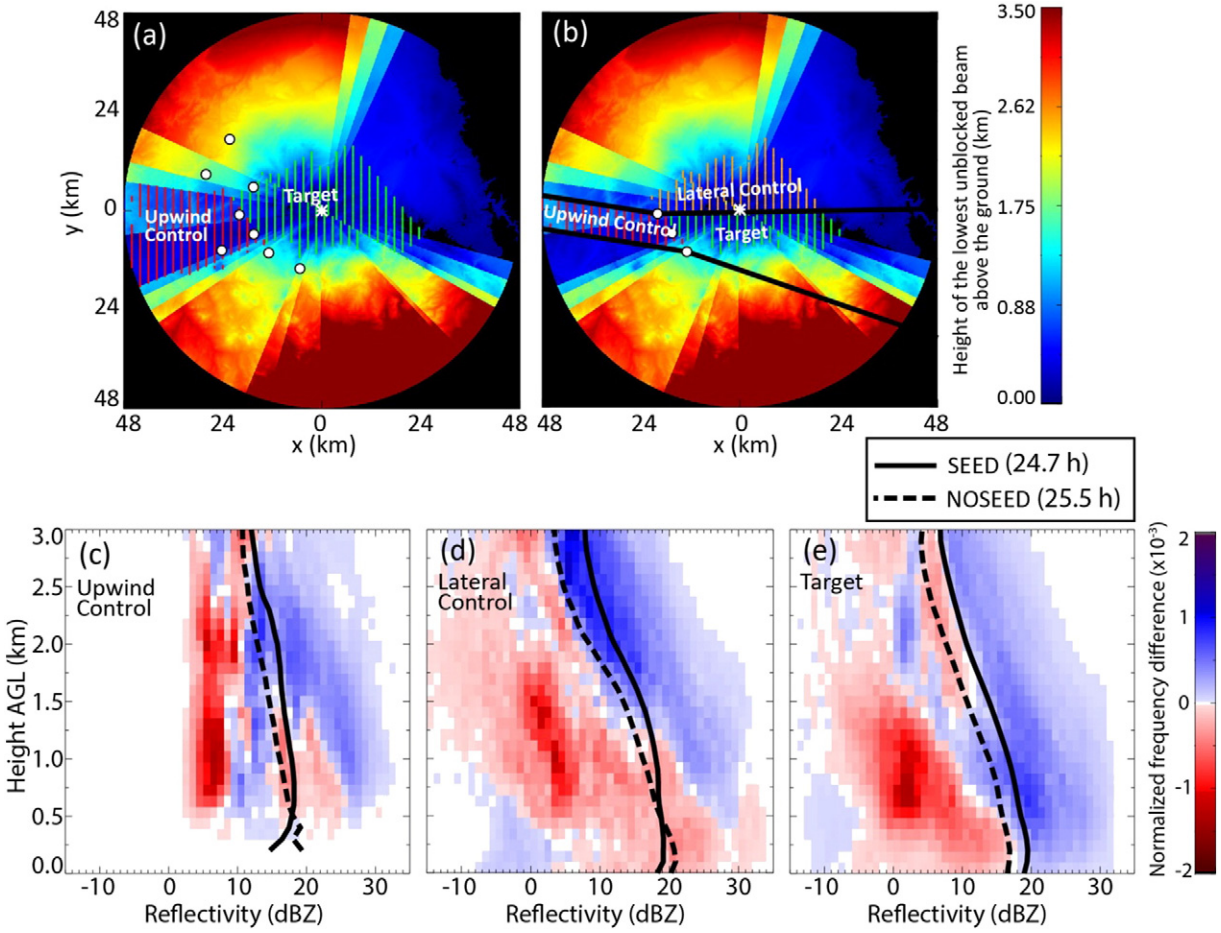

Fig. 8. Upper panels: height (km AGL) of the lowest unblocked DOW beam above the terrain of the SM. Also shown are the control and target regions for (a) all eight AgI generators and (b) the three core generators, for a given wind direction. Lower panels: DOW reflectivity difference FADs (SEED − NOSEED) for (a) the upwind control region (10 IOPs), (b) the lateral control region (subset of 5 IOPs), and (c) the target region (10 IOPs). Also shown in these panels are the mean reflectivity profiles during NOSEED and SEED.

region. The processing of the DOW data and the start and end times of NOSEED and SEED for all IOPs are described in Jing et al. (2015) and Jing and Geerts (2015). The DOW SEED and NOSEED periods are similar to those for the MRR and the gauges (Table 1), with adjustment for advection given the rather large target region.

Of the 12 IOPs over the SM (Table 1 in Part I), 10 were found to be suitable for DOW-based seeding impact analysis (Table 1). The two others (18-Jan. and 14-Feb. 2012) show no measurable echoes in the upwind control area during at least one of the periods (SEED or NOSEED), such that double differences cannot be calculated. Of the 10 good IOPs, three had convective echoes and seven had stratiform echoes only. All generators were used in three IOPs (Fig. 8a), and just the core generators (Fig. 8b) were used in the other seven (Table 1 in Part I). The wind direction was not suitable for a lateral control region to be defined in two of these seven IOPs, leaving just five IOPs.

The DOW reflectivity difference FADs (SEED − NOSEED) are shown separately for the two control regions and the target region in Fig. 8c–e. Storms generally show a trend towards stronger echoes during SEED. Below 1 km AGL, there is no net change (mean reflectivity values match) in both control regions, but not in the target region. In fact the blue–red dipole, with higher (lower) chances of high reflectivity values during SEED (NOSEED), is strongest in the lowest 1 km in the target region.

3. Change in ice particle concentration

3.1. Ice particle concentrations at the surface

As discussed in Section 2.5, the AgI plume likely reached the Battle Town site in eight IOPs in ASCII-12. Data from a Parsivel disdrometer at this site for these eight IOPs is partitioned into two periods (NOSEED and SEED, Table 1). The resulting ice particle size distribution data are composited in frequency-by-diameter-displays (FDDs) (Fig. 9). An FDD shows the normalized probability of a concentration of particles within a certain size bin. The mean particle concentration (solid line in Fig. 9a or b) tends to drop off exponentially with size, as expected. A bimodal distribution is apparent, with a secondary peak of small-particle concentrations an order of magnitude larger than the main peak, during SEED and especially during NOSEED. An FDD difference plot (Fig. 9c) shows a lower concentration of particles of all sizes (larger than ~300 μm) during SEED. This implies a lower reflectivity during SEED. This is not consistent with the FAD of the Battle Town site MRR (Fig. 7a), which shows a slightly higher reflectivity during SEED at the lowest level. But the MRR composite only spans six IOPs (Table 1). In both missing IOPs (18 and 19 January) the Parsivel concentration of especially larger ice particles is lower during SEED than NOSEED. Yet because the snowfall is light and shallow in both of these IOPs, the exclusion of these two IOPs (not shown) does not make the Parsivel SEED–NOSEED comparison consistent in sign with the MRR comparison at Battle Town site (Fig. 7a).

The sensitivity of the results can be quite sensitive to the number of IOPs available, especially when no control data are available. An example is the 28a-Feb. IOP (Table 1), which experienced a deep cloud (~5–6 km deep) with intense snowfall during NOSEED, and then clouds only half as deep with lighter snowfall and almost no large aggregates during SEED. Exclusion of this IOP (not shown) yields a more positive SEED − NOSEED difference for both Parsivel and target MRR. Ideally a second "control" Parsivel would have operated simultaneously on the mountain crest, but away from the AgI plumes. As discussed in Part I (Section 3.1), all available IOPs (except two, with changes in weather conditions during the IOP) are included. The number of IOPs differs from probe to probe, depending on data availability and evidence for suitable wind (Section 2.5).

3.2. Ice particle concentrations at flight level

Flight-level data generally are not useful to examine the impact of ground-based seeding, since the typical flight level was 610 m above the highest terrain in the SM and the MB. (This is the lowest permissible flight level in clouds.) But since convective clouds carry PBL air towards the cloud top, the probability is higher that the AgI-impacted snow reaches flight level in convective clouds. Also, compared to the disdrometer on the ground, flight-level ice particle concentrations are not contaminated by blowing snow, and the smallest particle size measurable by a Cloud Imaging Probe (CIP) is about one order of magnitude smaller than for a disdrometer. Therefore we examine the flight-level CIP and 2DP data for the convective IOPs in ASCII-12 and ASCII-13. We excluded those IOPs without CIP data (during pre-ASCII), those when the CIP became ice-covered, and those with a higher-than-minimal flight level. That leaves just four "good" convective IOPs.

The flight tracks most likely impacted by ground-based seeding are legs 4 and 5, which are over and just downwind of the mountains crest, respectively (Fig. 1). They were flown 1.0 km AGL (1.2 km AGL) for leg 4 (leg 5). As before (Section 2.2), we separate these tracks in two parts, a region downwind of the AgI generators and a lateral control region (schematic insert map in Fig. 10). The CIP and 2DP measured ice particle concentrations are larger during SEED downwind of the AgI generators compared to NOSEED for these convective cases (Fig. 10a). The ice crystal concentration is higher only in smaller size bins ($D < 400$ μm, CIP data), but in larger size bins ($D > 1$ mm) both CIP and 2DP data show a lower ice concentration during SEED downwind of the AgI generators (Fig. 10a). Effectively the mean snow particle size decreases by a factor of ~two during SEED, in convective clouds downwind of the AgI generators. [The NOSEED:SEED mean diameter ratio is 1.44 (2.54) for the CIP (2DP).] A larger ice concentration of smaller ice particles is not observed in the lateral control region (Fig. 10b) during SEED: both CIP and 2DP data indicate no significant change in size distributions from NOSEED to SEED outside the "cone" (Fig. 10b). A similar difference in ice size distribution between target and lateral control sections on legs 4 and 5 is not observed in the seven stratiform cases with suitable data (not shown).

4. Precipitation impact

4.1. Definition of a double difference parameter

Case studies (Pokharel et al., 2014a, 2014b, 2015) and model simulations (*e.g.*, Chu et al., 2014) suggest that the difference in reflectivity vertical structure between NOSEED and SEED is largely due to natural storm variability, even in a rather steady storm. Some of the natural trend can be removed by considering the nearby trend over the same time, in an untreated area. Pokharel et al. (2014a) devise an expression of reflectivity change in the target area, relative to that in a control area. They define the radar reflectivity impact parameter (ZIP) as the difference between the temporal change (SEED − NOSEED) in average reflectivity (in dBZ units) in the target region and that in the control region, *i.e.*

$$ZIP = \Delta dBZ_T - \Delta dBZ_U \quad (2)$$

where $\Delta dBZ = dBZ_S - dBZ_N$, and subscript S (N) refers to SEED (NOSEED), while subscript T (U) refers to treated or target (untreated or control).

This ZIP can be expressed as a relative change in precipitation rate (R, mm h^{-1}), if we assume a relationship between R and Z (mm^6 m^{-3}). Pokharel et al. (2014a) define the precipitation impact factor (PIF) as a

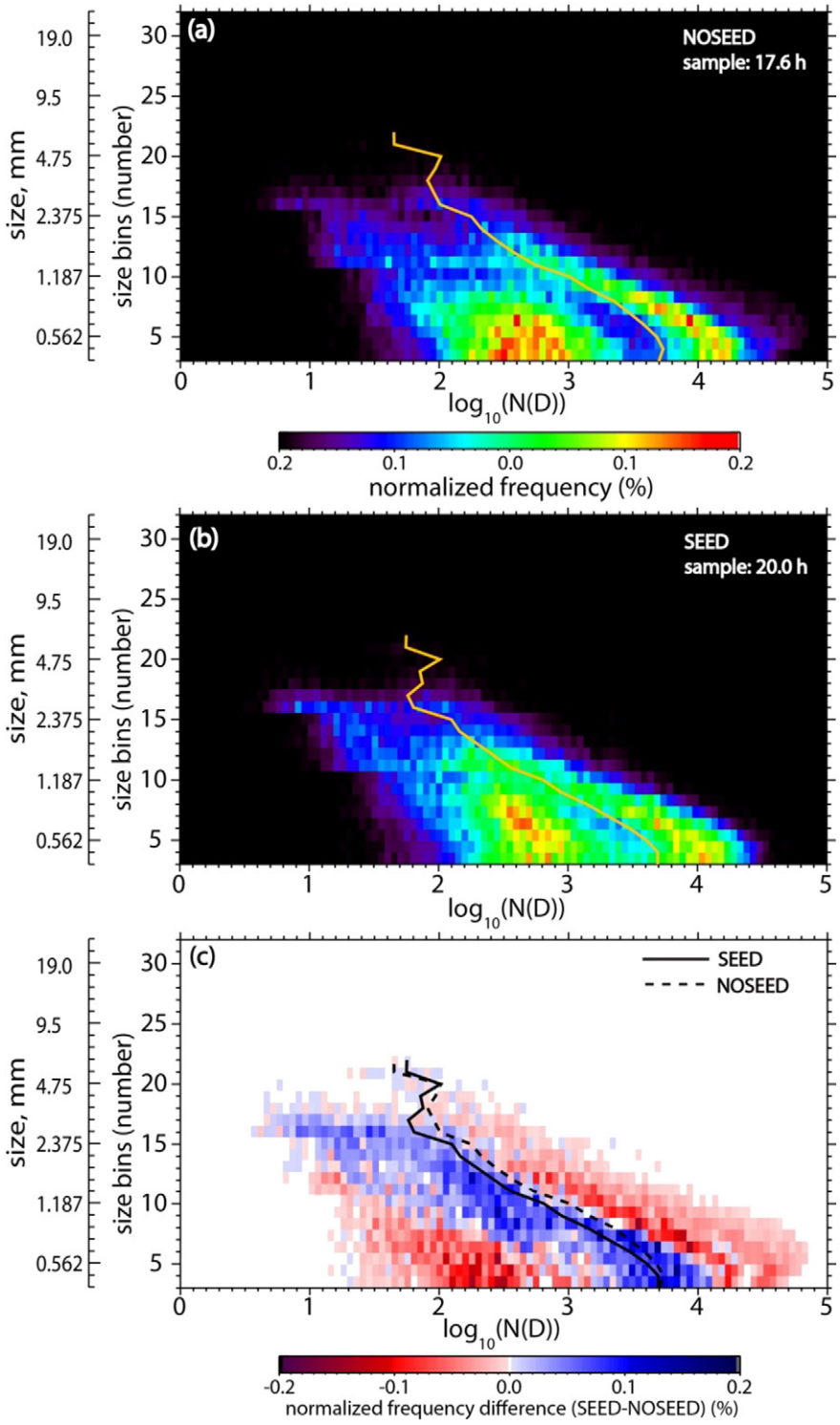

Fig. 9. Normalized frequency-by-diameter display (FDD) of snow particle concentration measured by a Parsivel disdrometer at Battle Town site during (a) NOSEED and (b) SEED, composited for eight ASCII-12 IOPs (Table 1). Panel (c) shows the difference (SEED minus NOSEED). The solid yellow lines in (a) and (b) show the average value; these lines are repeated as black lines in (c).

relative change in R (SEED vs. NOSEED) in the target area compared to the same relative change in the untreated area, *i.e.*

$$PIF = \frac{\frac{R_{S,T}}{R_{N,T}}}{\frac{R_{S,U}}{R_{N,U}}} \tag{3}$$

Assuming the standard Z–R relationship of the form $R = aZ^b$, where a and b are constants, PIF is related to ZIP as follows (Pokharel et al., 2014a):

$$PIF = 10^{\left(\frac{b \times ZIP}{10}\right)} \tag{4}$$

We use the value $b = 0.58$ for the WCR (Matrosov, 2007; Pokharel and Vali, 2011) and $b = 0.67$ for the MRRs and DOW (Matrosov et al.,

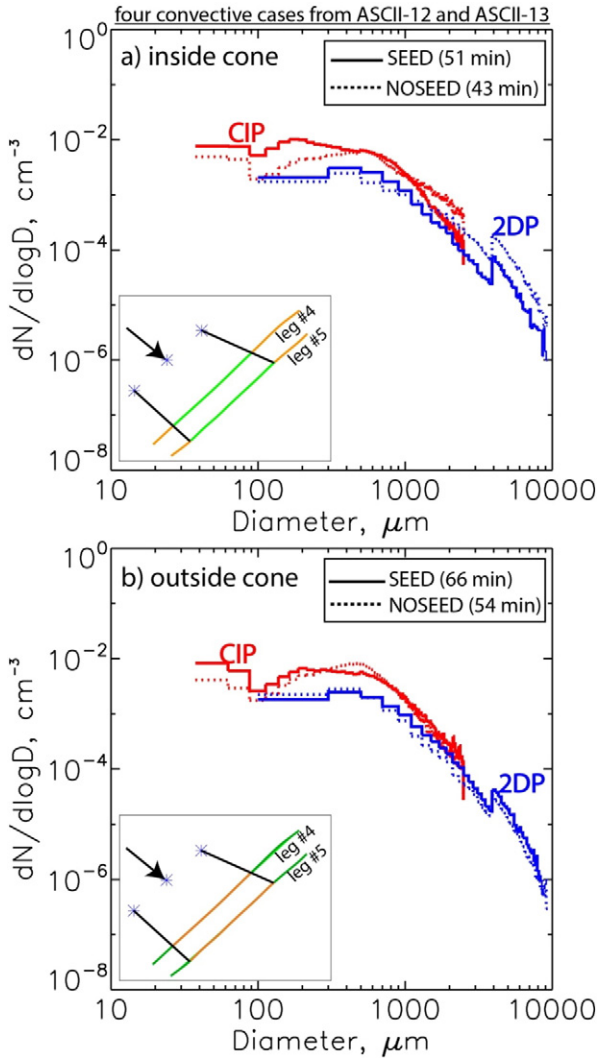

Fig. 10. Ice particle size distribution measured by the CIP (red) and the 2DP (blue) at flight level during SEED (solid) and NOSEED (dotted) along legs 4 and 5. The data come from the four convective IOPs with tracks at the minimum flight level; a) within the assumed AgI dispersion region (shown as green flight sections in the insert schematic map) and b) outside this region. This region varies with the mean wind direction for each IOP.

2009). A ZIP (PIF) value of zero (one) implies the same trend in the target and control areas, *i.e.* the AgI seeding is neutral.

4.2. Double difference uncertainties

There are two uncertainties with this approach. First, a double difference, *i.e.* the trend in a target area compared to the trend in a control area, only removes the natural trend if reflectivity or precipitation rate is strongly correlated (*e.g.*, Gabriel, 1999). ZIP (as defined in Eq. (2), with the upwind foothills area as control and the high-mountain region as target) can be interpreted also as the change in orographic enhancement from the NOSEED to the SEED period. The correlation between target and control is examined for all NOSEED periods in Part I (Section 6).

The second uncertainty regards the *Z–R* relationship, especially for snow. Various studies have shown considerable uncertainty for cm-wave radars (*e.g.* Fujiyoshi et al., 1990). The uncertainty is even larger for mm-wave radars when some hydrometeors are large enough to scatter in the Mie regime (>0.6 mm for W-band), as is the case here (Fig. 9) (Matrosov, 2007; Geerts et al., 2010; Pokharel and Vali, 2011). AgI seeding can change the size distribution of scatterers, *e.g.* it can result in more numerous small particles yet fewer large ice particles, as is suggested by some flight-level data (Section 3.2). In some scenarios this may increase *R* yet decrease *Z*. Given this uncertainty, we focus on observed changes in *Z* rather than radar-derived precipitation rate.

4.3. Snow gauge analysis

As part of the Wyoming Weather Modification Pilot Project (WWMPP), surface precipitation was measured using different types of gauges during ASCII (Breed et al., 2014). The gauge data were quality-controlled as described in Thériault et al. (2012). The most reliable snow gauges proved to be the ETI (Environmental Technology, Inc.) gauges. Two target sites are averaged for the SM, at Battle Pass and at HY-47 (Highway 47), located 4 km to the east (Fig. 1). The target site for the MB range is GLEES. All IOPs are listed in the last two columns of Table 1. Snow gauges were deployed upwind of the AgI generators, but these often recorded no measurable or significant snowfall during the IOPs, which are rather short. Therefore a lateral control is assumed for the PIF calculation from gauge data: identical snow gauges were deployed at Elk River and Chimney Park (Fig. 1). These sites are rather far to the south, out of reach of AgI contamination, but still over the respective mountain ranges. Good ETI gauge data, with wind blowing from a suitable direction, are available simultaneously at the control and target sites for 11 ASCII IOPs (Table 1). These gauge data are partitioned into NOSEED and SEED, to calculate a PIF value for each IOP according to Eq. (3).

4.4. Seeding impact on radar reflectivity and snowfall

The ZIP (or PIF) can only be calculated for datasets with both target and control measurements. This excludes the Parsivel altogether. For the MRR pair, it excludes select IOPs, *i.e.* two without upstream control MRR data (Table 1) and three with poor wind direction, such that the AgI plumes likely missed the target MRR at Battle Town site (Fig. 6). For the WCR, it excludes three pre-ASCII flights without leg 1 data, which are used as (upstream) control (Fig. 1). The number of remaining IOPs is listed in Table 2 for the various instruments. The ZIP values are calculated for these IOPs, based on average reflectivity from the lowest level AGL to 500 m AGL for the WCR, from the lowest level AGL to the highest layer below 1500 m AGL for the DOW. For the MRR, it is simply the lowest level with uncontaminated data for both probes, representing the layer 0.45–0.60 km AGL. Different instruments have their own target and control regions, SEED/NOSEED times, and different measurement principles, so ZIP values from different probes for the same IOP cannot be expected to be the same. PIF values corresponding to given ZIP values are not shown for the WCR and MRR in Table 2, simply because the *Z–R* relationship is even more uncertain for shorter-wavelength radars (Section 4.2). The DOW PIF values in Table 2 are computed from instantaneous low-level precipitation estimates. In other words, the DOW radar essentially is a surrogate precipitation gauge: precipitation rate is estimated at grid point resolution for each individual spatially interpolated DOW volume scan and then accumulated over the period of interest, and averaged in the region of interest. This approach is more accurate, since the *Z–R* relationship is not linear. The upwind control area for the DOW is based on more IOPs, than the lateral control area, but autocorrelation maps indicate that the latter correlates better with the target region (Section 6 in Part I), therefore results for both control regions are shown in Table 2.

The ZIP values averaged for all available IOPs are summarized in Table 2. *All instruments indicate an increase in Z (or precipitation rate) in the target region during seeding, compared to the trend in the control region.* ZIP values are positive for all but two of the SM cases according to both WCR and DOW data. The DOW-based ZIP/PIF values for the upwind control region are about the same as those for the lateral control region on average, as can be surmised from Fig. 8c–d. The verdict is more divided for the MB range, with positive WCR-based ZIP values

Table 2
Average reflectivity impact parameter (ZIP) and precipitation impact factor PIF (mean and standard deviation) for all available IOPs, based on different probes. R is the average liquid equivalent precipitation rate during NOSEED. ΔR is the average change in precipitation rate based on the PIF estimate. The variability between IOPs is highlighted by stating the mean ± the standard deviation.

Instrument	Control region	Mountain range	# of IOPs	ZIP (dB)	PIF	R (mm h^{-1})	ΔR (mm h^{-1})
WCR	Upwind	Both ranges	21	1.76 ± 5.25			
		SM	9	3.29 ± 6.46			
		MB	12	0.62 ± 3.72			
MRR	Upwind	SM	6	1.1 ± 8.2			
DOW	Upwind	SM	10	0.92 ± 2.73	1.14 ± 0.32	0.47	0.07
	Lateral	SM	5	0.91 ± 0.74	1.10 ± 0.09	0.57	0.05
Precipitation gauges	Lateral	Both ranges	11		1.57 ± 1.01	0.58	0.33
		SM	6		1.73 ± 1.02	0.64	0.47
		MB	5		1.38 ± 1.09	0.53	0.20

for eight IOPs, negative values for three IOPs, and no effect on the remaining flight. Only one (out of five) and two (out of six) IOPs has a negative gauge-based-PIF over the MB and SM ranges, respectively. In general, *the variation in ZIP/PIF values between IOPs is almost as large as its mean value*. This uncertainty partly may be attributed to differences in seeding efficacy, related to variables such as cloud temperature and LWP, examined below. There is also a significant measurement uncertainty: the data may not be representative of the true seeding impact. The ZIP estimate includes both a seeding impact and a difference in natural trend between target and control regions. It is impossible to discriminate between these two contributions. Also, aliased sampling (*e.g.*, a precipitation cell may miss a gauge or a WCR transect in one period and traverse it in another) may have a significant effect because the SEED and NOSEED periods are rather short. The DOW radar volume data, collected at rather high time resolution (10 min), may be the most representative of the areal mean precipitation rate in the target and control regions. In fact the standard deviation of ZIP/PIF is rather small for the DOW IOPs, at least for the lateral control (Table 2).

The relative change in precipitation is rather large, ranging from 10 to 14% according to the DOW to 57% for the snow gauges (Table 2). A modelling study of one of the ASCII cases (18 Feb. 2009) indicates a seeding-induced change of just 10%, when averaged over a target area comparable to the WCR flight tracks (Chu et al., 2014). The fractional change is large also compared to findings from several randomized seeding experiments, *e.g.*, a 14% increase for the 2005–09 Snowy Precipitation Enhancement Research Project (SPERC) in Australia (Manton and Warren, 2011), and 3–17% for the 2008–14 WWMPP, depending on the case selection criteria (Rasmussen, 2014). The large fractional change may be related to the rather light precipitation in ASCII IOPs, $R < 1$ mm h^{-1} on average (Table 2). Also shown in Table 2 is the expected change in precipitation rate (ΔR) based on the PIF estimate, *i.e.*

$$\Delta R = R\,(PIF - 1) \tag{5}$$

The average ΔR listed in Table 2 is based on values for each individual IOP, not the average PIF for all IOPs. ΔR ranges between 0.05 and 0.5 mm h^{-1}, depending on the instrument, which is a little smaller than the SPERC. (ΔR is larger for the gauge data, because of an outlier PIF estimate over the MB range.) So while the fractional change in snowfall is high for the ASCII cases, compared to randomized seeding experiments, the absolute change is not because of ASCII's focus on light orographic precipitation.

4.5. Profiles of ZIP

The impact of ground-based seeding is expected to remain within the turbulent PBL, which is 0.5–0.8 km deep in most ASCII IOPs, according to WCR vertical velocity spectra (Geerts et al., 2011). Deeper mixing may occur when convection is present over the target region. But the (mostly shallow) convective cells observed in ASCII tend to naturally precipitate mostly in the lee of the mountain (Jing and Geerts, 2015), and thus the seeding effect may be felt mostly further downwind than leg 5 or Battle Town site, the location of the target MRR (Fig. 1). The target region for the DOW does extend further in the lee (Jing et al., 2015). In short, the attribution of positive ZIP values to AgI seeding is more likely if these positive values are concentrated in the lowest ~1 km AGL. ZIP estimates become less reliable with height because there are fewer echoes aloft (*e.g.*, "data presence" lines in Fig. 2).

Profiles of ZIP for the three radar systems are shown in Fig. 11. The average ZIP profile, based on all available IOPs, does show positive values in the lowest 1 km, and near-zero values aloft for the WCR (green line in Fig. 11c). Positive values decrease with height also for the DOW, at least up to 2 km, above which level the data density becomes sparse and the ZIP estimate is dominated by a fewer cases (Fig. 11d). The profile of MRR composite ZIP (Fig. 11d) also shows decreasing values with height, but these values are all negative above 1 km AGL. Of the three composite ZIP lines in Fig. 11d, the MRR line is the least "informed", since it is based on the fewest cases and on 1D data only, with some uncertainty about the location of the AgI plume relative to the downstream MRR site (Section 2.5).

Stratification by precipitation type (Table 1 in Part I) show that, at least for the WCR, ZIP peaks near the surface for stratiform clouds and peaks higher (just below 1 km AGL) for convective clouds (Fig. 11a). This is consistent with the shallower mixing of AgI nuclei in stratiform clouds, and for convective precipitation to be lofted more, with positive ZIP values mostly in the lee (Jing and Geerts, 2015). Stratification by fetch from the AgI generators (Fig. 11b) shows higher ZIP values near the surface at close fetch and over a greater depth at greater fetch. Here close fetch means 2.5 and 7.5 km, if the wind is normal to WCR legs 2 and 3 respectively, and the greater fetch refers to normal distances of 13 and 18 km to legs 4 and 5 respectively. Finally, stratification by mountain range shows a similar lapse of ZIP values with height over both mountains (Fig. 11c), but higher values over the SM, where sampled clouds tend to be warmer and have more supercooled liquid water (SLW) (see Part I).

4.6. Ambient and cloud conditions affecting precipitation impact

The ZIP (PIF) values for the three radar systems and for the ETI gauges are plotted against cloud and environmental parameters, to examine whether these parameters have a measurable impact on seeding efficacy (Fig. 12). Each symbol corresponds to one IOP; different symbols are used for different data sources. Whereas the DOW and MRR PIF profiles shown in Fig. 11d are derived from average Z values using Eq. (4) (resulting in the unique relation between ZIP and PIF in Fig. 11d), DOW and MRR PIF values in Fig. 12 are computed from instantaneous, local low-level precipitation estimates, as in Table 2. Such an approach is not meaningful for the WCR, since it is an airborne (moving) measurement, and thus no local time integral can be taken. Instead, WCR reflectivity values are averaged first (in Z units) over the flight legs covering the appropriate region and time for any IOP, and then ZIP and PIF are computed from Eqs. (2) and (4) respectively. The PIF

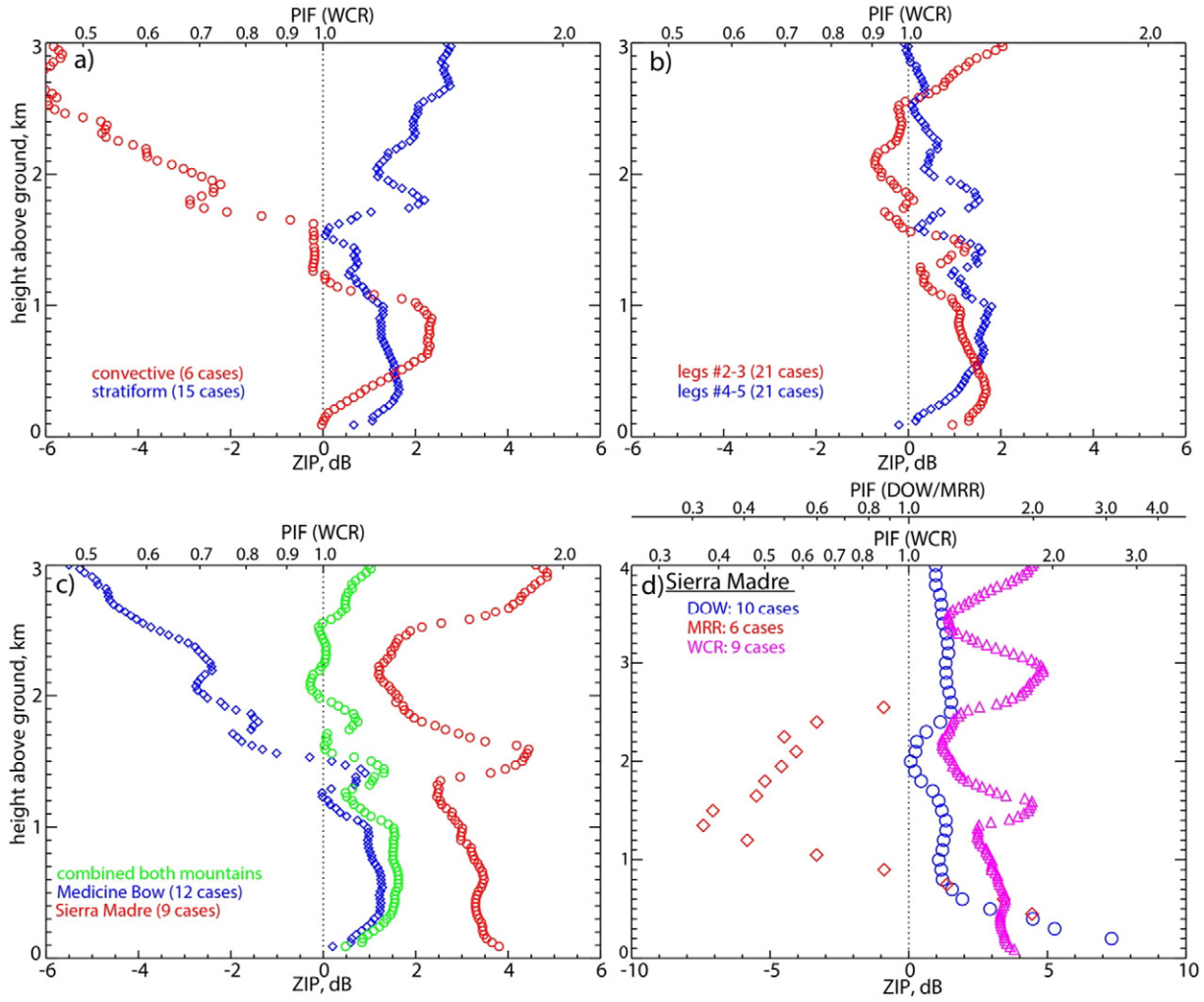

Fig. 11. Vertical profiles of WCR ZIP and PIF, based on composites of 21 flights partitioned in two parts, as follows: a) convective vs stratiform IOPs, b) short fetch (legs 2–3) vs long fetch (legs 4–5) target region, and c) MB vs SM. Panel (d) shows the ZIP and PIF profiles based on composite reflectivity for all available IOPs over the SM, according to data from three different radars.

scale on the right ordinate of each panel does not apply to the WCR, due to different ZIP–PIF relationships for mm-wave and cm-wave radars.

Lateral and upwind control values are shown separately for the DOW. The key parameter is cloud base temperature, as temperature controls AgI-induced ice nucleation in clouds. A cloud temperature significantly above about −7 °C may render AgI seeding ineffective, as the AgI activation (measured as the number of crystals yielded per gram of AgI) increases by 2.5 orders of magnitude between −6 and −10 °C (DeMott, 1997). But, as mentioned in the Introduction, seeding efficacy is constrained also at lower temperatures, ~−20 °C, depending on the concentration of natural ice nuclei. The ASCII IOPs do not reveal a significant relationship between ZIP/PIF and cloud base (LCL) temperature (Fig. 12a). ZIP/PIF values tend to be highest between −7 and −15 °C, but the average PIF for warmer cases (cloud base temperature > −7 °C is almost the same as that for colder cases. This may indicate that in most cases air parcels rise well above the LCL.

Deep orographic clouds with very cold cloud tops (below −25 to −30 °C) are not conducive to seeding because of ice initiation aloft and the seeder–feeder effect at lower levels (Manton and Warren, 2011; Manton et al., 2011; Grant and Elliott, 1974). Indeed ZIP ~ 0 (PIF ~ 1) for IOPs with a cloud top temperature below −25 °C (Fig. 12d), and PIF is larger for IOPs with a cloud top temperature above −25 °C, compared to cold cloud tops. Deeper clouds also tend to have smaller PIF (Fig. 12f), while PIF values are overwhelmingly large for shallow-cloud IOPs (cloud depth < 3.0 km), which dominate in ASCII.

The main driver for ice crystal growth and thus seeding efficacy is SLW content (Ryan et al., 1976), which tends to increase with temperature (Super and Heimbach, 2005). We do not find a clear relationship between ZIP/PIF and the liquid water path (LWP) (Fig. 12c), which is surprising. Maybe ASCII does not include enough cases with high LWP values.

The relative impact of seeding on precipitation rate is inversely proportional to the natural precipitation intensity in stratiform orographic clouds, according to modelling work (Xue et al., 2013). The reason is that ice crystals are naturally more abundant and SLW is consumed more efficiently in deeper, more intense storms. ASCII observations tend to confirm this, although the correlation is weak (Fig. 12e). Finally, a stronger cross-mountain wind tends to produce more SLW and thus more efficient seeding. But with fresh snow on the ground, surface winds exceeding ~10 m s^{-1} may produce blowing snow, which may serve as a natural ice crystal source from the ground up (Geerts et al., 2015b), overwhelming the effect of ground-based AgI seeding. In general, there is no significant relation between ZIP/PIF and wind speed (Fig. 12b).

None of the relationships shown in Fig. 12 are statistically significant at the $p = 0.05$ level. ASCII measurements are inadequate to gain insights into how key cloud and environmental parameters impact seeding efficacy. This may be because the relationship between relative precipitation change and these parameters is complex, and controlled by other factors such as natural ice nucleus concentration, which we

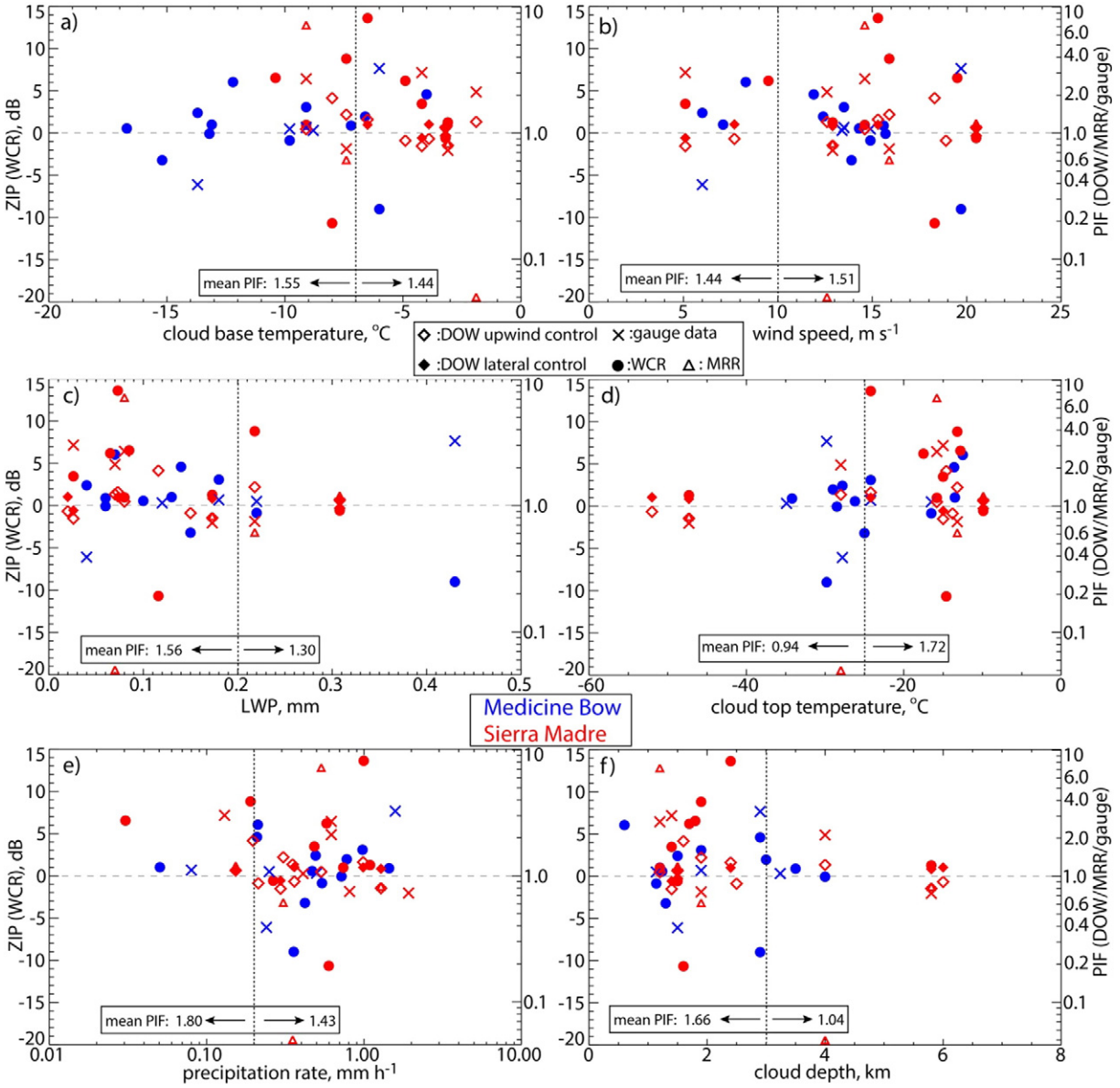

Fig. 12. Variation of reflectivity impact parameter (ZIP) and precipitation impact factor (PIF) with ambient and cloud conditions, based on four instrument types (three radar and one gauge), each with their own target and control region(s), and each with their own largely overlapping but not identical SEED/NOSEED periods and available IOPs, located over the MB (blue) or the SM (red) ranges. The horizontal dashed line in all panels separates a positive effect (above) from a negative effect (below). The ZIP values are related to a) cloud base temperature, b) low-level mean wind speed, c) liquid water path, d) cloud top temperature, e) precipitation rate, and f) cloud depth. The vertical dotted lines separate different regimes. The mean PIF values for those regimes, based on all instruments/IOPs, are shown.

did not measure. It also reflects the uncertainty in ZIP/PIF estimation (Section 4.2).

5. Discussion

The data collected in ASCII allow a unique, in-depth exploration of precipitation changes in response to ground-based AgI seeding. Before summarizing the findings, we raise several caveats and suggestions for any future observational studies into glaciogenic cloud seeding:

- The biggest challenge remains natural variability (National Research Council, 2003; Garstang et al., 2005), thus the experimental design should include control regions or periods. These need to be representative, with strongly correlated precipitation records (*e.g.* simultaneous measurements laterally displaced over the same mountain range) yet uncontaminated. Each storm is different, and to address both the wide space of parameters (*e.g.* temperature, LWP, drop size distribution, cloud depth, and wind speed) and the aliasing inherent to relatively brief sampling in individual storms, *numerous cases are needed for physical process studies.* This statement is separate from any statistical argument about the number of cases needed for randomized experiments.
- *Caution is warranted in relating radar reflectivity changes to precipitation changes*. This study does not address how *Z–R* relations can change in response to seeding, due to changes in particle size distribution and/or particle density. Direct in situ or remote measurements of ice water content and snow density are desirable.
- This study also ignored variations in *concentrations of natural cloud-active aerosol* in the upstream airmass. Both cloud condensation nuclei and especially *ice nuclei should be measured.*
- *Freshly fallen snow at the target ground site should be chemically analyzed for trace elements including Ag and other co-varying minerals*, as

was done in ASCII-12 but not in other ASCII campaigns. This is because it offers the only confirmation that the falling snow is impacted by seeding. The more frequently falling snow can be sampled, the better. This may require a large sampling surface under light snowfall. The sampling should continue about 2 h after the AgI generator switch-off time to examine delayed impact.

- One of the challenges in windy cases is that *snow particles measured near the surface may originate from the ground or nearby trees*. We placed the in situ instruments on a scaffold a few meters above the snow surface in a tree-sheltered opening at Battle Town site. At the same time, they cannot be placed too high, since some instruments, like the hotplate and disdrometer, become unreliable under strong winds.
- *The surface target site needs to be selected carefully*, perhaps with the aid of detailed flow modelling over the target mountain. Battle Town site is more likely to be impacted by upwind ground-based seeding because of its location near a pass into which flow is channeled, especially under more stable conditions. On the other hand, GLEES is located behind the bulge of MB Peak situated on top of the MB plateau. GLEES is less suitable as stratified flow (and seeding-impacted snow) may be diverted around this bulge, whereas the air over that location often arises from aloft due to frequent downslope windstorms in the lee of MB Peak which rapidly sublimate snow (*e.g.*, Geerts et al., 2015a).
- The analysis of the impact of ground-based seeding is complicated by boundary-layer turbulence, ice crystal transfer from the ground up into cloud (Geerts et al., 2015b), and complex flow patterns around the terrain. Also, airborne cloud and precipitation probes are of limited use to examine ground-based seeding because the minimum flight level is rather high in clouds over complex terrain. Much progress can be made examining cloud microphysical processes following the *airborne injection of AgI nuclei*, preferably in stratiform orographic clouds. This has been done before (*e.g.*, Deshler et al., 1990), but not with novel cloud radar and in situ cloud probes.

6. Conclusions

This paper examines the impact of ground-based AgI seeding on snow growth in orographic clouds observed in southern Wyoming during ASCII. Reflectivity profiles were collected both upstream (control) and downstream (target) of the AgI generators from three radar systems, two profiling (WCR and MRR), and one volume-scanning (DOW). The impact of AgI seeding is isolated by contrasting the measurements collected before seeding commenced (NOSEED) against those during seeding (SEED), both in a target region and in a control region. Each period is about 2 h long, and is adjusted for advection depending on the location of the target relative to the AgI generators. The three radar systems and snow gauges are complementary in that they have their own target and control regions, measurement technique, vantage, and IOP array in the composite.

Data from all IOPs were included in the composite analysis, unless a significant change in weather occurred between NOSEED and SEED, the relevant instrument did not work, or the wind direction was wrong. For ASCII-12, a higher-than-expected Ag concentration in fresh snow samples collected at the target site (Battle Town site) during SEED was used also as an argument for effective targeting and inclusion of a dataset in the composite analysis.

The ASCII sample size is relatively small, with 21 IOPs for the WCR, 10 for the DOW, 6 for the MRR pair, and 11 for the snow gauges. Thus natural trends from NOSEED to SEED persist in the composite, *e.g.* storms naturally weakened during most of the ASCII-12 IOPs over the SM, but they tended to intensify from NOSEED to SEED in the IOPs over the MB. An attempt is made to remove the natural trend in each IOP by comparing the trend in the target region to that in the nearby control region. Thus double differences or double ratios are examined, such as the PIF, involving both a geographical and a temporal change. This reduces but does not remove uncertainties in attribution to AgI seeding.

The following conclusions emerge:

- All instruments indicate an increase in near-surface radar reflectivity (precipitation rate for gauges) in the target region during seeding, compared to the trend in the control region. The change is most pronounced at low levels, consistent with ground-based seeding. In relative terms, the increase is rather large, but this double difference/ratio (ZIP/PIF) varies significantly from IOP to IOP.
- Most of this variation relates to non-homogenous natural trends across the mountain range, and/or to unrepresentativeness of the measurements and the control region. In other words, signal detection in a noisy field such as precipitation remains the main challenge.
- The ASCII sample size is not adequate either to quantify the magnitude of the seeding impact on snowfall with confidence, or to identify the atmospheric and cloud conditions most suitable for ground-based seeding. The strongest signal is that clouds with warmer tops (>-25 °C) are more suitable for glaciogenic seeding.
- More numerous, but smaller ice crystals are observed in convective clouds downwind of the AgI generators at flight level (~1.1 km AGL) during SEED, compared to NOSEED. This change is not observed to the side of AgI plumes (lateral control region) in the same convective IOPs, nor in stratiform clouds. A Parsivel disdrometer located at the target site does not show such increase in ice crystal concentration during SEED.
- PIF values are larger for IOPs over the Sierra Madre compared to the IOPs over the Medicine Bow. This may be attributable to a higher cloud LWP and temperature over the former range, and/or to local topographic factors that control the flow to the target site.
- The ASCII project leaves room for improvements. Several suggestions are made to improve the experimental design of future cloud seeding research campaigns.

Acknowledgements

The ASCII campaign is funded by the National Science Foundation grant AGS-1058426. This work also received funding from the Wyoming Water Development Commission grant 1001552C and the United States Geological Survey grant 10000628S, under the auspices of the University of Wyoming Water Research Program. The operation of the AgI generators, the upstream MRR, and the microwave radiometer was supported by the WWMPP, which is funded by the State of Wyoming and managed by Barry Lawrence. We thank the crews of the UWKA and the DOW for working under often harsh conditions, Dan Breed for the MRR data collected at Ladder Livestock ranch, and Arlen Huggins for the trace analysis of snow samples collected at Battle Pass.

References

Breed, D., Rasmussen, R., Weeks, C., Boe, B., Deshler, T., 2014. Evaluating winter orographic cloud seeding: Design of the Wyoming Weather Modification Pilot Project (WWMPP). J. Appl. Meteorol. Climatol. 53, 282–299.

Chu, X., Xue, L., Geerts, B., Rasmussen, R., Breed, D., 2014. A case study of radar observations and WRF LES simulations of the impact of ground-based glaciogenic seeding on orographic clouds and precipitation: part I: observations and model validations. J. Appl. Meteorol. Climatol. 53, 2264–2286.

DeMott, P.J., 1997. Report to North Dakota Atmospheric Resource Board and Weather Modification Incorporated on Tests of the Ice Nucleating Ability of Aerosols Produced by the Lohse Airborne Generator. Dept. Atmos. Sci., Colorado State Univ., Report, Fort Collins, CO 15 pp.

Deshler, T., Reynolds, D.W., Huggins, A.W., 1990. Physical response of winter orographic clouds over the Sierra Nevada to airborne seeding using dry ice or silver iodide. J. Appl. Meteorol. 29, 288–330.

Fujiyoshi, Y., Endoh, T., Yamada, T., Tsuboki, K., Tachibana, Y., Wakahama, G., 1990. Determination of a *Z–R* relationship for snowfall using a radar and high sensitivity snow gauges. J. Appl. Meteorol. 29, 147–152.
Gabriel, K.R., 1999. Ratio statistics for randomized experiments in precipitation stimulation. J. Appl. Meteorol. 38, 290–301.
Garstang, M., Bruintjes, R., Serafin, R., Orville, H., Boe, B., Cotton, W., Warburton, J., 2005. Finding common ground. Bull. Am. Meteorol. Soc. 86, 647–655.
Geerts, B., Miao, Q., Yang, Y., Rasmussen, R., Breed, D., 2010. An airborne profiling radar study of the impact of glaciogenic cloud seeding on snowfall from winter orographic clouds. J. Atmos. Sci. 67, 3286–3301.
Geerts, B., Miao, Q., Yang, Y., 2011. Boundary-layer turbulence and orographic precipitation growth in cold clouds: evidence from profiling airborne radar data. J. Atmos. Sci. 68, 2344–2365.
Geerts, B., Yang, Y., Rasmussen, R., Haimov, S., Pokharel, B., 2015a. Snow growth and transport patterns in orographic storms as estimated from airborne vertical-plane dual-Doppler radar data. Mon. Weather Rev. 143, 644–665.
Geerts, B., Pokharel, B., Kristovich, D.A.R., 2015b. Blowing snow as a natural glaciogenic cloud seeding mechanism. Mon. Weather Rev. 143, 5017–5033.
Grant, L.O., Elliott, R.E., 1974. The cloud seeding temperature window. J. Appl. Meteorol. 13, 355–363.
Holroyd, E.W., McPartland, J.T., Super, A.B., 1988. Observation of silver iodide plumes over the Grand Mesa of Colorado. J. Appl. Meteorol. 27, 1125–1144.
Houze, R.A., 2012. Orographic effects on precipitating clouds. Rev. Geophys. 50, RG1001. http://dx.doi.org/10.1029/2011RG000365.
Huggins, A.W., 2007. Another wintertime cloud seeding case study with strong evidence of seeding effects. J. Weather Mod. 39, 9–36.
Jing, X., Geerts, B., 2015. Dual-polarization radar data analysis of the impact of ground-based glaciogenic seeding on winter orographic clouds. Part II: convective clouds. J. Appl. Meteorol. Climatol. 54, 2099–2117.
Jing, X., Geerts, B., Friedrich, K., Pokharel, B., 2015. Dual-polarization radar data analysis of the impact of ground-based glaciogenic seeding on winter orographic clouds. Part I: mostly stratiform clouds. J. Appl. Meteorol. Climatol. 54, 1944–1969.
Maahn, M., Kollias, P., 2012. Improved Micro Rain Radar snow measurements using Doppler spectra post-processing. Atmos. Meas. Tech. 5, 2661–2673.
Manton, M.J., Warren, L., 2011. A confirmatory snowfall enhancement project in the Snowy Mountains of Australia. Part II: primary and associated analyses. J. Appl. Meteorol. Climatol. 50, 1448–1458.
Manton, M.J., Warren, L., Kenyon, S.L., Peace, A.D., Bilish, S.P., Kemsley, K., 2011. A confirmatory snowfall enhancement project in the Snowy Mountains of Australia. Part I: design and response variables. J. Appl. Meteorol. Climatol. 50, 1432–1447.
Matrosov, S.Y., 2007. Modeling backscatter properties of snowfall at millimeter wavelengths. J. Atmos. Sci. 64, 1727–1736.
Matrosov, S.Y., Campbell, C., Kingsmill, D., Sukovich, E., 2009. Assessing snowfall rates from X-band radar reflectivity measurements. J. Atmos. Ocean. Technol. 26, 2324–2339.
National Research Council, 2003. Critical Issues in Weather Modification Research. National Academy Press (123 pp.).
Pokharel, B., Geerts, B., 2016. A multi-sensor study of the impact of ground-based glaciogenic seeding on clouds and precipitation over mountains in Wyoming. Part I: project description. Atmos. Res. 182, 269–281.
Pokharel, B., Vali, G., 2011. Evaluation of collocated measurements of radar reflectivity and particle sizes in ice clouds. J. Appl. Meteorol. Climatol. 50, 2104–2119.
Pokharel, B., Geerts, B., Jing, X., 2014a. The impact of ground-based glaciogenic seeding on orographic clouds and precipitation: a multi-sensor case study. J. Appl. Meteorol. Climatol. 53, 890–909.
Pokharel, B., Geerts, B., Jing, X., Friedrich, K., Aikins, J., Breed, D., Rasmussen, R., Huggins, A., 2014b. The impact of ground-based glaciogenic seeding on orographic clouds and precipitation: a multi-sensor case study. Atmos. Res. 147-148, 162–181.
Pokharel, B., Geerts, B., Jing, X., 2015. The impact of ground-based glaciogenic seeding on clouds and precipitation over mountains: a case study of shallow orographic cloud with large supercooled droplets. J. Geophys. Res. 120, 6056–6079.
Rasmussen, R., 2014. The Wyoming Weather Modification Pilot Project, level II study. Executive summary. Available at http://wwdc.state.wy.us/weathermod/WYWeatherModPilotProgramExecSummary.pdf.
Ryan, B.F., Wishart, E.R., Shaw, D.E., 1976. The growth rates and densities of ice crystals between −3 °C and −21 °C. J. Atmos. Sci. 33, 842–850.
Super, A.B., Heimbach, J.A., 2005. Feasibility of snowpack enhancement from Colorado winter mountain clouds: emphasis on supercooled liquid water and seeding with silver iodide and propane. Final Report. Technical Services Center, Bureau of Reclamation, Denver Federal Center, Denver, CO (63 pp.).
Thériault, J., Rasmussen, R., Ikeda, K., Landolt, S., 2012. Dependence of snow gauge collection efficiency on snowflake characteristics. J. Appl. Meteorol. Climatol. 51, 745–762.
Xue, L., Tessendorf, S., Nelson, E., Rasmussen, R., Breed, D., Parkinson, S., Holbrook, P., Blestrud, D., 2013. AgI cloud seeding effects as seen in WRF simulations. Part II: 3D real case simulations and sensitivity tests. J. Appl. Meteorol. Climatol. 52, 1458–1476.
Xue, L., Chu, X., Rasmussen, R., Breed, D., Boe, B., Geerts, B., 2014. The dispersion of silver iodide particles from ground-based generators over complex terrain. Part II: WRF large-eddy simulations vs. observations. J. Appl. Meteorol. Climatol. 53, 1342–1361.
Yuter, S., Houze, R.A., 1995. Three-dimensional kinematic and microphysical evolution of Florida cumulonimbus. Part II: frequency distributions of vertical velocity, reflectivity, and differential reflectivity. Mon. Weather Rev. 123, 1941–1963.